Advances in Water Resources 144 (2020) 103705

Contents lists available at ScienceDirect

Advances in Water Resources

journal homepage: www.elsevier.com/locate/advwatres

Longitudinal dispersal properties of floating seeds within open-channel flows covered by emergent vegetation

Xiaoguang Liu[a], Yuhong Zeng[a,*], Gabriel Katul[b,c], Wenxin Huai[a], Yu Bai[a]

[a] State Key Laboratory of Water Resources and Hydropower Engineering Science, Wuhan University, Wuhan 430072, China
[b] Nicholas School of the Environment and Earth Sciences, Duke University, Durham, NC, USA
[c] Department of Civil and Environmental Engineering, Duke University, Durham, NC, USA

ARTICLE INFO

Keywords:
Floating seed
Emergent vegetation
Hydrochory
Seed-vegetation collision
Dispersion mechanism
Longitudinal dispersal

ABSTRACT

The effect of emergent stems on the transport of downstream floating particles (e.g., buoyant seeds) is explored theoretically and experimentally at moderate to high Reynolds number ($R_d = 2U_b a_s/\upsilon > 300$) in an open channel, where U_b is the bulk velocity, a_s is stem radius, and υ is the kinematic viscosity. Longitudinal dispersion (D_l) of such seeds is shown to be given by $D_l = U_p^3 \tau_0^2 \eta(1-\eta)/2/(S_1 + \eta\tau_0 U_p)$ thereby requiring the bulk transport velocity of particles U_p, spacing between canopy elements S_1, collision efficiency η between a particle and the stem, and a wake trapping time scale τ_0. Linkages between U_p and U_b, and terms η and τ_0 are then derived using inhomogeneous flow characteristics adjacent to the stem with physical properties of particles. A semiempirical model with potential flow theory around the stem is introduced to estimate η whereas τ_0 is shown to be related to the bulk drag coefficient and radius of stems. The D_l is experimentally determined across a wide range of R_d and particle sizes and shown to be in good agreement with the proposed model calculations.

1. Introduction

Seed dispersal by water (hydrochory) sets a spatial template for the spread, structure and survival of many aquatic plants (Nilsson et al., 1994; Merritt and Wohl, 2006; Defina and Peruzzo, 2010; Cunnings et al., 2016; Liu et al., 2018). It is one of the main processes responsible for regeneration and self-sustaining rehabilitation of riparian ecosystems (Schneider and Sharitz, 1988; DeWoody et al., 2004; Hyslop and Trowsdale, 2012). Dispersal by wind (anemochory) has received significant research attention and mathematical treatment (e.g., Okubo and Levin, 1989; Greene and Johnson, 1996; Clark et al., 1998; Levine, 2003; Katul et al., 2005; Nathan et al., 2011; Duman et al., 2016); however, hydrochory has received disproportionately less attention. One complication arising in hydrochory that is absent in anemochory is the need to distinguish between non-buoyant and buoyant seeds. Buoyant seeds can be transported through the combined action of flowing water, surface waves and even surface wind (Nilsson et al., 1994). Many aquatic plant seeds have the ability to float, meaning that an extended floating time enhances dispersal distances by mean advection (Danvind and Nilsson, 1997; Nilsson et al., 2010; Riis and Sand-Jensen, 2006). A number of models use empirical or semi-empirical approaches to describe seed transport in the form of a so-called dispersal kernel (Groves et al., 2009; Shi et al., 2020). Dispersal kernels represent the probability of finding a seed at some finite distance from the parent source. Empirical approaches describe plausible mathematical shapes for the dispersal kernel that are then used to predict distribution of herbaceous plants and their communities (Levine, 2003). Mechanistic approaches, such as the semi-empirical Gaussian plume equations have also been used to describe dispersal kernels using mean velocity and hydraulic geometry as variables (Groves et al., 2009). The outcome from such models is that the majority of seeds deposit near the release point but few seeds can spread over long distance highlighting the possibility of long-distance dispersal by a small number of seeds. These results have been used to justify the differing dispersal patterns of short- and long-distance transport from parent source of seeds, as has been observed in wind dispersal studies (Nathan et al., 2002).

Another mechanism that can lead to differing dispersal patterns near- and far- from the parent source or release point is vegetation capture or trapping. Floating seeds can be captured temporarily or permanently by vegetation and mathematical models accommodating such capture are now beginning to receive theoretical and experimental attention. Defina and Peruzzo (2010) proposed a stochastic model to describe the transport and diffusion of floating particles and the trapping mechanisms by emergent flexible vegetation with varied plant density. They adopted a weighted combination of two exponential distributions to predict the distribution of particle retention time (Defina and Peruzzo, 2012). These two distributions were intended to reflect retention time differences for short- and long-duration trapping events. Further-

* Corresponding author.
E-mail address: yhzeng@whu.edu.cn (Y. Zeng).

https://doi.org/10.1016/j.advwatres.2020.103705
Received 16 November 2019; Received in revised form 23 July 2020; Accepted 25 July 2020
Available online 29 July 2020

more, Peruzzo et al. (2012) investigated the effect of surface tension on the fate of floating particles dispersal in open channel flows with emergent vegetation at low Reynolds number and confirmed the effectiveness of such a weighted scheme. Liu et al. (2018) further explored the mechanisms responsible for floating particles dispersal in slow-moving flow with emergent vegetation by combining kinematic and statistical models of particle-stem interactions. These prior efforts primarily dealt with particle collision and trapping by stems due to surface tension at low flow velocity (analogous to a small Weber number, e.g., Peruzzo et al., 2012; Liu et al., 2018). However, for moderate to high Reynolds numbers, surface tension between stems and particles may be small and even ignored (i.e. high Weber number). Dispersal mechanism of such floating particles and corresponding particle-stem interaction at moderate to high Reynolds numbers have rarely been investigated, however, which may terminate long-distance transport and change the fate of floating seeds within vegetated riverway. The work here attempts to fill this knowledge gap through novel theories and flume experiments. The focus is on the interaction between floating particles and emergent stems in fast-moving free surface flows in which collision and trapping events exist but not due to surface tension.

When passing through an array of stems at moderate to high Reynolds number, the trajectory of a floating particle is impacted by a number of flow features:

i. The particle transport velocity U_p is significantly larger than the bulk flow velocity U_b due to the so-called "blockage effect", which was first proposed by Maskell (1963) and developed by Zdravkovich (2003).
ii. The stems generate wake turbulence and mechanical dispersion that distort the particle trajectory from streamlines set by the mean flow in the vicinity of the stem.
iii. The stems modify particle trajectory when a collision occurs that can lead to rebound or trapping.

These mechanisms form the basis of a newly proposed model for floating particle dispersion in uniformly distributed array of emergent rigid stems. The main novelties of the proposed approach include a semiempirical kinematic model with potential flow theory to estimate the probability of collision between particles and the stem; and a retention time model based on wake theory following an isolated collision event, by combining with classical theories of blockage effects within an array of cylinders, we can arrive at a formulation for the longitudinal dispersion coefficient of floating particles at high Reynolds number. By dispersion coefficient, we mean the coefficient that describes the spatial spread of a cloud of particles over a sufficiently long time interval as conventional in Lagrangian particle studies (Fischer, 1973). Moreover, it is to be noted that dispersal mechanism within the array of stems of floating seeds differs from the well-studied solute particles (e.g., chemical contaminant, biological hormone) and suspended fine particles (e.g., sediments), i.e. "surface effect", hydrodynamic processes that occur at a free water surface (e.g., wind drag and surface tension effects); and "volume effect", inertial impaction, sidewise repulsion (due to asymmetric attached lateral velocity induced by stems acting on floating particles and lateral pressure on the side away from the centre of stem). "Volume effect" can be significant for floating seeds but not necessarily for small grains or sediments. Accordingly, the length scale ratio between floating seeds and partices are expected to become a dynamically significant factor primarily because of "volume effect" and "surface effect".

2. Theoretical model

To explore the canonical aspects of floating seed dispersion for emergent canopy flow at high Reynolds number, the flow is assumed to be steady and uniform with the water surface not subjected to any wind stresses or wave action. The vegetation covering the channel bottom is composed of a honeycomb stem arrangement (Fig. 1). The stems are rigid, cylindrical in shape with radius a_s, and are characterized

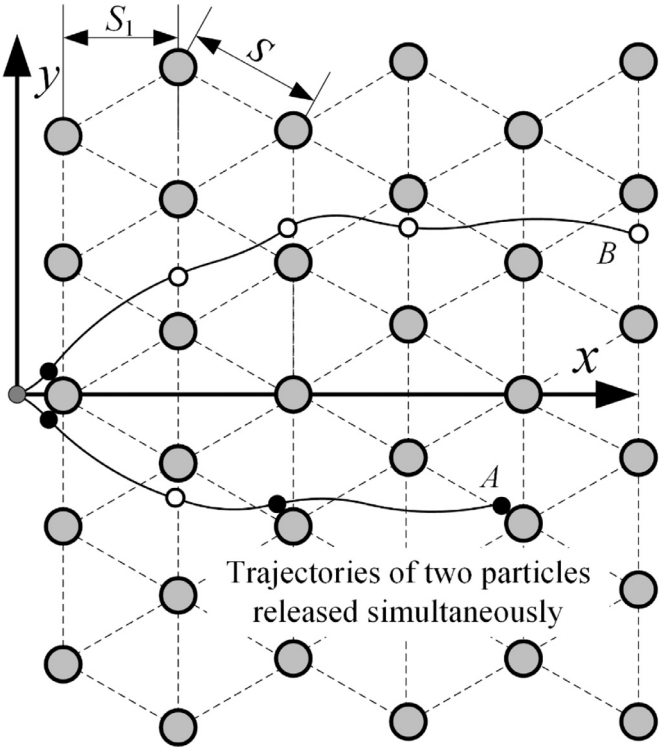

Fig. 1. Schematic of the honeycomb arrangement for a uniformly distributed array of stems. The two particles (A and B) are released simultaneously and take different paths within the array of stems due to the obstruction by stem elements. The mean flow is from left to right.

by a uniform stem density n_s defined by the number of stems per unit ground area, or the solid area fraction $\lambda = \pi n_s a_s^2$. Wooden spherical particles are used to represent the floating seeds for consistency with prior experiments (Defina and Peruzzo, 2010, Peruzzo et al., 2012 and Liu et al. 2018). For the arrangement in Fig. 1, two distances are pointed out: the center-to-center spacing between adjacent stems, $S = 1/\sqrt{n_s}$; and the length of each segment in the direction of the mean flow, $S_1 = 0.5\sqrt{3/n_s}$ (see Fig. 1).

2.1. Longitudinal dispersion

The dispersal of floating particles within such a stem array is anisotropic and is determined by two mechanisms: wake turbulence and mechanical dispersion (Nepf et al. 1996). In Fig. 1, two floating particles (A and B) starting at the same position will migrate within the stem array along different trajectories and experience longitudinal separation during a fixed time interval. Particles traversing a distance S_1 in the direction of the flow may collide with a stem with the collision efficiency η, defined as the ratio of upstream width of particles colliding with the stem to the center-to-center spacing between adjacent stems. After the collision, a particle encounters a backflow region and resides in the wake for some time, and then it moves into an intermediate wake region. Let τ_0 be the mean retention time due to an isolated collision and temporary wake trapping event (compared to no-collision case). Define N_t as the total number of segments a particle passes through the entire vegetated patch and N_i as the total number of collisions a particle experiences after crossing N_t segments. By definition, the entire length of the vegetated patch is $N_t S_1$. The total retention time a particle experiences while passing through the entire vegetated patch length is $\tau_r = \tau_0 N_i$. Thus, the probability distribution function of τ_r, labeled as $q(\tau_r)$, when a particle traverses the total distance $N_t S_1$ is,

$$q(\tau_r) = C_0 \tau_0 \eta^{N_i} (1-\eta)^{N_t - N_i}, \quad (1)$$

where C_0 is the binomial coefficient. The probability of τ_r is based on a binomial distribution with a mean time and a variance$\sigma_t^2 = \tau_0^2 N_t \eta(1-\eta)$ as discussed elsewhere (Defina and Peruzzo, 2010). When a cloud of particles is released at the same position, the total time that the cloud of particles experiences longitudinal separation is:

$$t_m = \frac{N_t S_1}{U_p} + N_t \eta \tau_0, \tag{2}$$

where U_p is the bulk transport velocity of the particle. The first term in Eq. (2) describes the absence of collision and wake distortion scenario, whereas the second term accommodates the collision and wake trapping effects on the overall travel time. Thus, the longitudinal spatial variance of the cloud can be estimated as:

$$\sigma_l^2 = U_P^2 \sigma_t^2 = U_p^2 \tau_0^2 N_t \eta(1-\eta) \tag{3}$$

At very long times, the longitudinal dispersion of the cloud will converge to a Fickian diffusion (by the central limit theorem) so that the longitudinal spatial variance of the cloud grows linearly with t_m. Under those (asymptotic) conditions, the longitudinal dispersion coefficient can be defined from$\sigma_l^2 = 2D_l t_m$ (Rutherford, 1994), or

$$D_l = \frac{\sigma_l^2}{2t_m} = \frac{U_p^3 \tau_0^2 \eta(1-\eta)}{2(S_1 + \eta \tau_0 U_p)}. \tag{4}$$

To estimate D_l requires determining parameters$\tau_0$and η as well as links between bulk velocity U_b and particle transport velocity U_p. In the applications of dimensional analysis, identifying all the variables impacting the sought quantity is the most challenging step (Katul et al., 2019), herein, it is instructive to ask to what degree can τ_0 and η be predicted from dimensional analysis. That is, the list of plausible variables impacting τ_0 may include processes relevant to inertial impaction, the buoyancy of the particles, and the size of the wake zone trapping the particle. Hence, this plausible list leads to

$$\tau_0 = f_1(U_b, a_p, a_s, L_w, \rho_p, \rho_w), \tag{5}$$

where $f_1(\cdot)$ is an unknown function to be determined, a_p and a_s are the particle and stem radius, respectively (arising from inertial impaction), $\rho_p$and$\rho_w$are densities of the particle and water (arising from buoyancy), L_w is length scale of the wake zone, combined with U_b, can be used to form a characteristic trapping time scale in the wake zone behind the stem. Introducing the following dimensionless groups$a_r = a_p/a_s$and$\rho_r = \rho_p/\rho_w$, dimensional analysis alone can be used to reduce the list of variables to

$$\tau_0 \propto a_r^{m_1} \rho_r^{m_2} L_w/U_b \tag{6}$$

Here, dimensional analysis cannot determine the exponents m_1 and m_2. The length scale of the wake zone (=L_w) is further impacted by the wake generation process so that$L_w \sim a_s C_{ds}$, with C_{ds} being the bulk drag coefficient of the stem. Eq. (6) can then be rearranged as

$$\tau_0 \propto C_{ds} a_r^{m_1} \rho_r^{m_2} a_s/U_b \tag{7}$$

Likewise, the collision efficiency η must, at minimum, depend on the spacing between the interfaces of stem elements (i.e.,$S_1 - a_s$) and the size of the particle passing between these stem elements. These two distances can be combined to yield

$$\eta \propto 2a_p/(S_1 - a_s) \tag{8}$$

The proposed model next aims at describing τ_0 and η using what is known about the flow field around cylinders, which can then be used in conjunction with Eq. (4) to predict D_l.

2.2. Collision model

At low Reynolds number, the collision efficiency, η, primarily depends on the acceleration caused by surface tension that draws floating particles toward stems. As the bulk flow velocity increases, the effect of particle inertia caused by advection will be dominant in a collision with

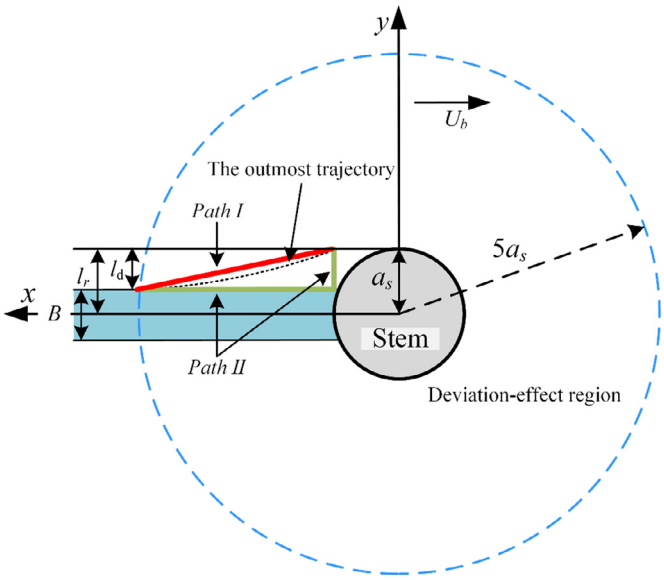

Fig. 2. The outmost trajectory of the downstream particle (dotted line) approaching the stem within the Deviation-effect region, B is upstream width of particles colliding with the stem, path I and II (thick line) denote the extreme paths of collision.

stems. Similar to Liu et al. (2018), the Weber number ($W_b = 2\rho_w U_b^2 a_p/\sigma$, with σ as the surface tension) is introduced to assess the vegetated water bodies, for the small-scale issue of floating particles, when $W_b >> 1$, the effect of surface tension on interactions between floating particles and emergent stems can be ignored. In a flow through a dense population of emergent stems, the blockage effect will also alter the flow around a stem. It was found that the presence of the stem reduces the cross-sectional area locally and results in a concomitant increase in the velocity around the body in relation to the bulk flow velocity (Zdravkovich, 1997). In a flow through a dense population of emergent stems, streamlines become circuitous as they bend and branch around the stem (Nepf et al., 1997), a downstream floating particle approaching a stem will be subject to a lateral acceleration that acts to push the particle away from the stem. The acceleration is caused by lateral velocity difference between particles and attached lateral velocity due to fluid parcels are displaced laterally by the presence of stems in the corresponding cross-sections. The frequency of random events that directly collided particles are pushed away from stems are called 'deviation effect'. Britter et al. (1979) measured turbulence around a circular cylinder and discussed how streamlines and turbulence are distorted relative to the upstream state. The most pertinent result from this analysis is that there exist a region of vorticity distortion near the cylinder surface that is roughly $5a_s$. In this region, distortions from the free streamlines became apparent and the attached lateral velocity has a significant effect on the transport of particle. Thus, a circular region with a radius of $5a_s$ can be used to delineate the zone sensing such deviation-effects (see Fig. 2).

Let l_r and l_d be defined as lateral lengths of direct collision and the deviation effect, respectively. Considering downstream particles initially entering the deviation-effect region and defining a variable $\xi = y - (l_r - l_d)$, a semiempirical kinematic model can be developed to determine this acceleration. Based on numerical simulations in a confined pipe at a microfluidic scale, Di Carlo et al. (2009) describes the lateral repulsive force acting on particle due to asymmetrical distribution of flow velocity and pressure as $F_l \propto \rho_w U_b^2 a_p^2 (a_p/L_c)^4$ when the particle moving near the rigid boundary, L_c is the characteristic length, and F_l is inversely proportional to distance to the rigid boundary, their results are of important reference value in quantifying the lateral repulsive force between particles and rigid boundary (the stem) though the

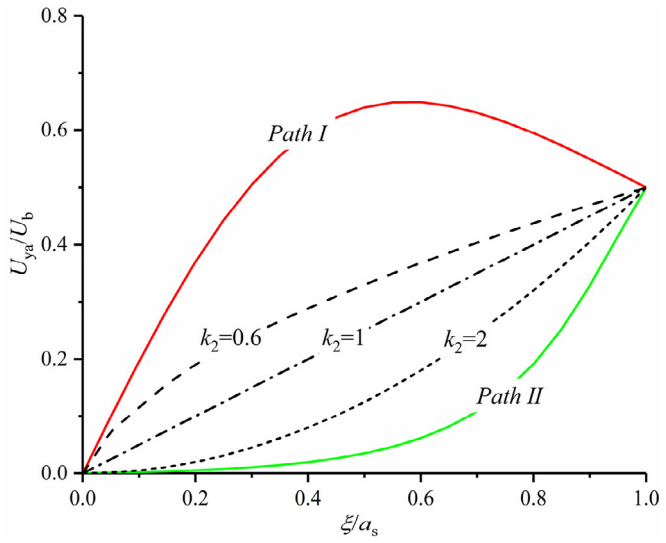

Fig. 3. Lateral velocity the collided particle experiences for paths I and II, and three potential particle trajectories (corresponding k_2 = 0.6, 1, 2).

experimental situation was quite different from present study. Because of similar mechanisms of F_l and lateral fluid drag acting on particle, the former is integrated to the latter, and considered into the lateral deviation of particle, both of which depend directly on the distribution of attached lateral velocity around the upstream half of the stem. In a real flow, separation occurs on the upstream half of stems and the inviscid solution may be a reasonable approximation to the real flow there, thus, the attached lateral velocity can be approximately $U_{ya} = \frac{2U_b x y a_s^2}{(x^2+y^2)^2}$. In terms of the outmost trajectories (Fig. 2), path I denotes the shortest route or minimum U_{ya} the particle experiences and path II denotes the longest route or maximum U_{ya} the particle experiences. The presupposed particle trajectory is between paths I and II, and corresponding attached lateral velocity the particle experiences is weighted value of both, herein, a power-law function with variable ξ is proposed to describe the weighted value,

$$U_{ya} = k_1 U_b (\xi/a_s)^{k_2} \tag{9}$$

where k_1 and k_2 are scale and shape parameters, respectively, and k_2 varies according to different downstream particle trajectory, as shown in Fig. 3, three dotted lines (k_2=0.6, 1, 2) denote different potential particle trajectories. Intuitively, the greater value of k_2 suggests that the outmost trajectory will be much closer to path II, and the smaller value of which will be much closer to path I. Analogous to definition of Palmer et al. (2004), herein, the evaluation of inertial impaction for floating particle is defined as the ratio of the stopping distance to stem radius,

$$S_{tf} = a_r^2 \rho_r R_d / 9\delta_a \tag{10}$$

where a_r is particle to stem ratio, ρ_r is the specific gravity of particle and δ_a is the area submergence or the ratio between the submerged and whole projected area of the particle. A classical kinematic equation is established for particles to evaluate the deviation effect in rectangular coordinates, which is,

$$\begin{cases} m_p \frac{d^2\xi}{dt^2} = \frac{1}{2}\rho_w A_p C_{dp} U_{ys}^2 \\ m_p \frac{d^2x}{dt^2} = \frac{1}{2}\rho_w A_p C_{dp} U_{xs}^2 \end{cases}, \tag{11}$$

where U_{ys} and U_{xs} are y and x-components of the slippage velocity between the particle and fluid parcels; m_p is the mass of a particle and $m_p = 4\pi a_p^3 \rho_p/3$; $A_p = \delta_a \pi a_p^2$, and the C_{dp} is the drag coefficient for the floating particle in turbulent fluids. Before the collision occurs with regard to the outmost trajectory of the downstream particle approaching the stem, x-component of the slippage velocity between the particle and fluid parcels is close to zero, i.e., $U_{xs} \approx 0$, meanwhile, due to the elapse time from entering the deviation-effect region ($\xi = 0$, $x \approx 5a_s$,$t = 0$) to colliding with the stem ($\xi = l_d, x = a_s$, $t = t_e$) is relatively short, U_{ys} is approximately equal to U_{ya}.

Combining with Eq. (9 and 11) can be rearranged as

$$\begin{cases} m_p \frac{d^2\xi}{dt^2} = \frac{3\delta_a}{8a_p}\frac{\rho_w}{\rho_p} C_{dp} U_b^2 k_1^2 (\xi/a_s)^{2k_2} \\ m_p \frac{d^2x}{dt^2} = \frac{1}{2}\rho_w A_p C_{dp} U_{xs}^2 \end{cases} \tag{12}$$

As previously discussed by Liu et al. (2019), the specific gravity of particle may be interpreted as the relative submergence volume when the particle floats on the water surface. As a particle approaches the stem, if the lateral deviation distance is less than l_d when reaching the position x=a_s, the particle will collide with the stem. Thus, the boundary condition on Eq. (12) is given as,

$$\begin{cases} t = 0 \begin{cases} \xi = 0 \\ \frac{d\xi}{dt} = 0 \end{cases} \\ t = t_e \begin{cases} \xi = l_d \\ U_{ya} = 0.5 U_b \end{cases} \end{cases} \tag{13}$$

therefore, the solution to Eq. (12) is

$$l_d = \frac{3a_s C_d}{4a_r}\frac{\delta_a}{\delta_v}(2k_2 + \frac{4}{2k_2+1} - 3). \tag{14}$$

A dimensionless shape coefficient$\gamma = \delta_a/\delta_v$is proposed for a floating particle herein, with δ_v the ratio between the submerged and total volume, which is negatively and positively correlated with the density and sphericity of particles, respectively. As flow velocity increases, the deviation effect will be more significant, thus, the collision efficiency η depends on the rate of particle inertia and the deviation effect and can be described as,

$$\eta = \frac{B}{S} = \frac{2(a_s - l_d)}{S} \tag{15}$$

2.3. Wake trapping model

After a particle collides with a stem, the velocity of the particle instantaneously drops to zero; subsequently, the particle slips into the wake behind the stem and finally drift into the free stream. The time that a particle spends during the whole collision process along the longitudinal length of the free stream is defined as retention time. Each particle will experience a varying number of collisions (i.e., temporary trappings) as it passes through the array of stems, and the retention time of temporary trapping is random and described by a probability distribution model. Thus, both the number of collisions and the corresponding retention time are random variables that determine D_l. For stems that are uniformly distributed with nearly identical trapping performance, any two collision events are not linked and the probability distribution of the retention time for collision events is memoryless (Defina and Peruzzo, 2010). The large-scale behavior of retention time due to collisions obeys the exponential distribution and relates to the angle of particles enter the retention zone, which was verified in numerical experiments (Ziemniak et al., 1994) and laboratory studies (Defina and Peruzzo, 2010). As R_d increases (R_d > 300), the steady recirculation vortex behind the stem begins to shed and turbulence gradually contributes to the downstream wake. Within the array of emergent stems, Kiya et al. (1980) suggested the transition from laminar to turbulent wake structure may be delayed toR_d = 200. For conditions of fully developed turbulence, form drag between upstream and downstream sides of the stem due to turbulent wake structure dominates the drag force acting on the stem (Thom, 1933). It follows that the bulk drag coefficient is assumed to be positively related to the characteristic velocity deficit and length scale of wakes. To evaluate the effect of turbulence wake

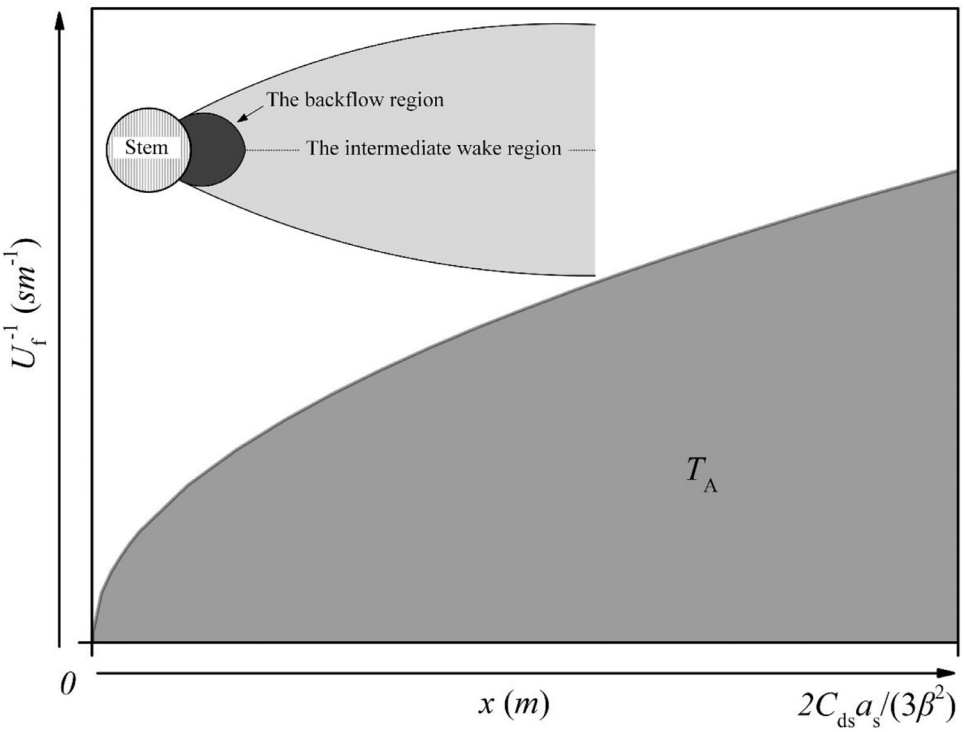

Fig. 4. Variations of U_f^{-1} with increasing x, where T_A is the area integral from x=0 to $2C_{ds}a_s/3\beta^2$ along the centerline of the intermediate wake region.

on retention time, the velocity deficit U_f in the wake should be quantified. The measured velocity profiles along the center line of the wake converge well to accepted wake theory (Zdravkovich, 1997),

$$U_f = U_b\sqrt{\frac{5C_{ds}a_s}{81\beta^2}}x^{-0.5} \tag{16}$$

whereβ = O(1)is a correction coefficient and herein the velocity deficit U_f along the centerline of the wake is used to assess the acceleration of a collided particle in the wake. The U_f^{-1} is plotted as a function of x in Fig. 4 and the time a particle resides in the wake regions (mainly for the intermediate wake region) is given by the integral from $x\rightarrow 0^+$ to $x = 2C_{ds}a_s/3\beta^2$, corresponding to U_f/U_b = 30%, which is defined as the marginal value of the intermediate wake region (Zavistoski, 1994), and represents the distribution feature of velocity deficit in whole wake,

$$T_A \propto \int_{x\rightarrow 0^+}^{x=2C_{ds}a_s/3\beta^2}\sqrt{\frac{81\beta^2}{5C_{ds}a_s}}\frac{\sqrt{x}}{U_b}dx \approx \frac{4\sqrt{2}}{\sqrt{15}}\frac{C_{ds}a_s}{U_b\beta^2} \tag{17}$$

The time T_A can be regarded as a parameter to evaluate the effect of turbulence wake on retention time (i.e. $\tau_0 \propto T_A \propto C_{ds}a_s/U_b$). Eq. (17) is commensurate with predictions from dimensional considerations alone. After the collision occurs, the downstream particles will accelerate from zero to the bulk transport velocity within the wake region, in the case of qualitative analyses of the acceleration, particle inertia (the mass or specific gravity) and area of the intermediate wake are positively correlated with the retention time, and the larger stems produce larger wake scale, i.e., $\tau_0 \propto \rho_r/a_r$. Thus, $\tau_0$can be written as $\tau_0 \propto (C_{ds}a_s/U_b)(\rho_r/a_r)$, and$(C_{ds}a_s/U_b)(\rho_r/a_r)$is defined as the retention parameter. To define the retention time of an isolated collision event, the trajectory of a particle within the array of stems is divided into two segments, or the 'delayed' and 'smooth' transport segments (see Fig. 5). The T_{de} is the time spent by the particle to pass through the length of the delayed transport segment, L_{de}. The U_{sm} is the particle transport velocity in the smooth transport segment across gaps among stems if no interactions with the vegetation occur. The retention time during an isolated collision event$\tau_0$can now be described as

$$\tau_0 = T_{de} - L_{de}/U_{sm} \tag{18}$$

This completes the derivation of τ_0 and η from what is known about inertial particle flow past an isolated cylinder at moderate to high Reynolds number. Using the derived models for τ_0 and η, the proposed formulation for D_l is now compared against experiments.

3. Experimental method

Laboratory experiments were conducted in a rectangular flume that is 18 m long, 1.0 m wide, and 0.5 m deep with glass walls to permit optical access. To maintain an approximately uniform flow rate in the flume, a tailgate located at the exit of the flume was used. The recirculating flow rate (Q) was measured by an electromagnetic flowmeter, the bulk velocity U_b was calculated as the ratio of Q to flowing area within the array. A uniform array of rigid clean cylindrical wooden dowels with diameter of 0.6 cm and height of 25 cm were used to represent the canopy. The cylinders were uniformly inserted on polyvinyl chloride boards to create a test section that was 4 m long. Wooden sphere of different sizes (radii set to 0.4 cm, 0.3 cm, and 0.2 cm) were used to represent buoyant seeds. All particles were evenly painted with white dye to improve image tracking capabilities. The cylinders protruding out of the water surface were small enough (less than 3cm) so that trapped particle cannot cover the image during recording. For each experiment, a total of sixty particles were released one by one 50 cm upstream of the test section (see Fig. 6) and at random positions in the transverse direction.

All the experimental runs were recorded by a digital camera (sampling frequency is 25 *Hz*) mounted over the flume, and can move left or right to alter recording position. As shown in Table 1, two sets of experiments were performed to test different aspects of the model. One set fixes the stem density but varies the bulk velocity. The other set varies the stem density but fixes the bulk velocity. Setup labeled *A1* to *A7* use seven different U_b ranging from 0.065 to 0.219 m/s for a fixed stem density of 1366 m^{-2} (the bulk velocity). This setup was intended to explore the effect of flow velocities on the collision efficiency between particles and the stem. Setup labeled *B1* to *B4* includes four different stem density (n_s ranges from 554 to 1164 m^{-2}) and used particle sizes a_p=0.3 cm but a fixed bulk velocity U_b = 0.113 ms^{-1}. This setup was intended

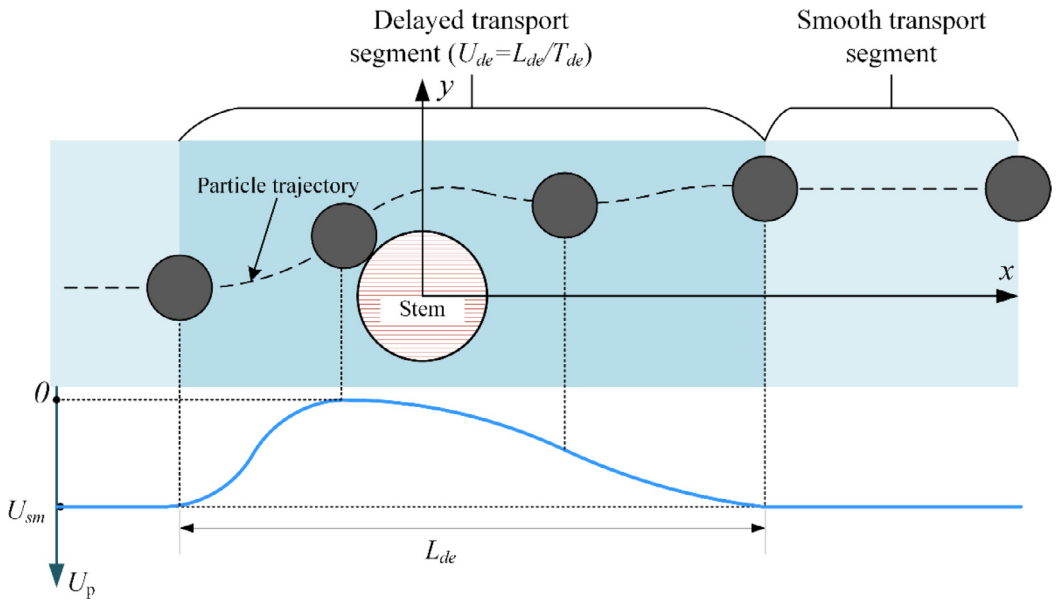

Fig. 5. Schematic of a particle trajectory of collision with the stem in the delayed and smooth segments with varying U_p. Flow is from left to right.

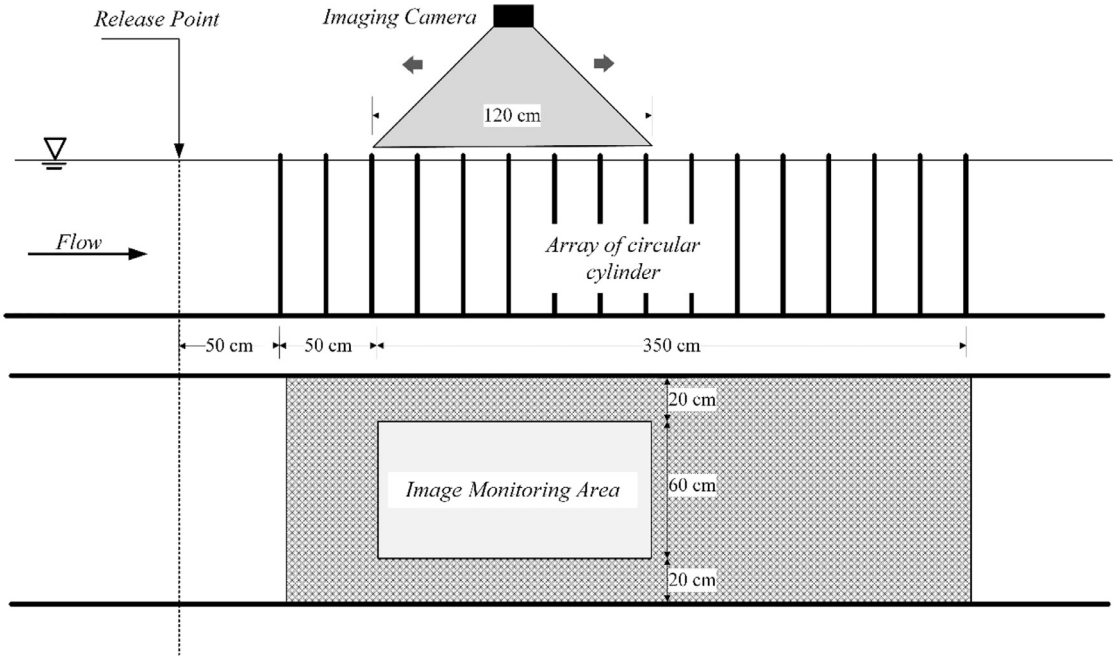

Fig. 6. Lateral (the above) and top (the below) views of the experimental setup in the flume. Mean flow is from left to right.

Table 1
Summary of the experimental setup highlighting the Reynolds number, the stem density, and particle sizes for each run.

Experiments	U_b (m/s)	R_d	W_b	S (cm)	n_s (m^{-2})	λ	Types of particles
A1	0.0645	387	0.5699-0.7979	2.706	1366	0.0386	0.2, 0.3, 0.4cm
A2	0.0894	536	1.0949-1.5328	2.706	1366	0.0386	0.2, 0.3, 0.4cm
A3	0.113	678	1.7492-2.4488	2.706	1366	0.0386	0.2, 0.3, 0.4cm
A4	0.138	828	2.6088-3.6523	2.706	1366	0.0386	0.2, 0.3, 0.4cm
A5	0.163	978	3.6396-5.0954	2.706	1366	0.0386	0.2, 0.3, 0.4cm
A6	0.190	1140	4.9452-6.9233	2.706	1366	0.0386	0.2, 0.3, 0.4cm
A7	0.219	1314	6.57-9.198	2.706	1366	0.0386	0.2, 0.3, 0.4cm
B1	0.113	678	2.099	4.250	554	0.0157	0.3cm
B2	0.113	678	2.099	3.727	720	0.0204	0.3cm
B3	0.113	678	2.099	3.272	934	0.0264	0.3cm
B4	0.113	678	2.099	2.931	1164	0.0329	0.3cm

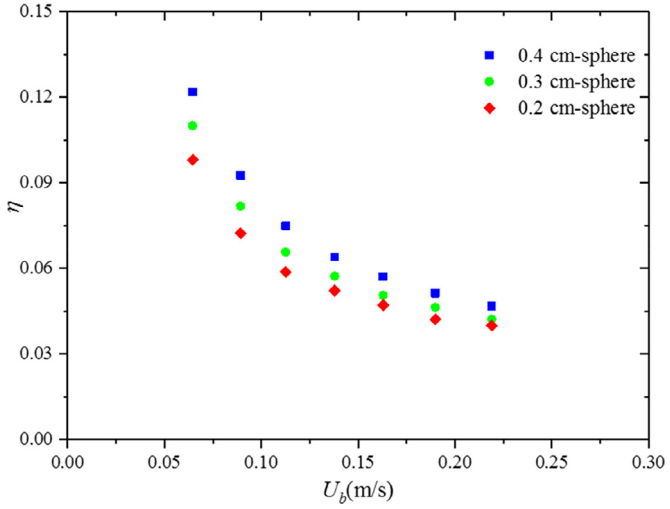

Fig. 7. Variation of the collision efficiency η with the bulk flow velocity U_b for all three sphere sizes.

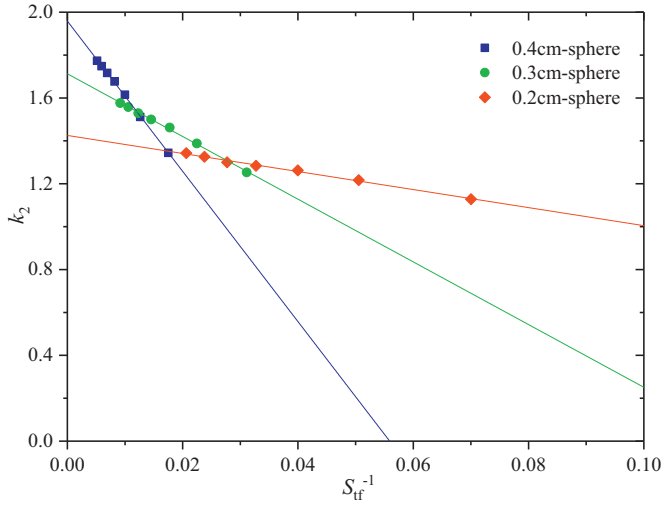

Fig. 8. Variation of parameter k_2 with the dimensionless parameter S_{tf} for all three sphere sizes.

to explore the effect of stem densities on D_l of floating particle. By analyzing the recorded video of particle tracking using the video analysis software Image-Pro Plus 6.0 (Media Cybernetics, Silver Spring, USA), particle trajectories within the monitoring window (see Fig. 6) were analyzed. The number (N_i) of measured collision events were determined from stable decelerating process and minimal particle velocity approximate to zero, the bulk transport velocity of the particle (U_p) can also be directly determined. The bulk transport velocity of the particle (U_p) can also be directly determined. As a particle passes through the array of stems, the total number of interaction points N_t using the measured path length X is $N_t = 1 + X/S_1$; thus, the measured collision efficiency η can be estimated as follows:

$$\eta = N_i/(1 + X/S_1) \tag{19}$$

4. Result and discussion

4.1. Collision efficiency

In this study, a kinematic model was used to describe the collision and quantify the relation between the collision efficiency and the flow velocity and particle characteristics. Runs *B1-B7* are to be used for exploring the performance of the proposed model. With measured collision events within the image monitoring area and using Eq. (19), the collision efficiency can be obtained and plotted as a function of U_b as shown in Fig. 7, η reduces as U_b increasing and basically meet the negative logarithmic relationship. Defina and Peruzzo (2012) suggested that the collision efficiency is likely to be independent of vegetation pattern and density. Liu et al., (2018) further developed the model and concluded that η depends mainly on the flow velocity and particle physical characteristics.

The shape parameter k_2 can now be determined by combining the data of (η, U_b) pairs with Eqs. (12–14). The results are featured in Figs. 7 and 8. As shown in Fig. 8 and discussed in section 2.2, k_2 has a significant linear correlation with the inverse of S_{tf}, S_{tf}^{-1}, the intercept and slope of curves depend on "volume effect", specifically, a_r. For wooden spheres of different sizes, multiparameter nonlinea fitting is used to obtain the empirical formula of k_2 with R_d,

$$k_2 = -163a_r/R_d + 1.713\sqrt{a_r} \tag{20}$$

the slope denotes effect of "volume effect" on the deviation of trajectories, the larger particle means more significant deviation, predictably, k_2 becomes a small constant as a_r decreases to 0.1.

Comparison between calculated from Eq. (20) and measured k_2 is presented in Fig. 9, with coefficient of determination $R^2 = 0.988$. As the importance of inertial impaction increases, i.e., a larger value of S_{tf} for floating particle, the outmost trajectories of collided particles will gradually divert close to path II (Fig. 3), and the dominant deviation effect will make downstream particles much easier to escape away from stems. One could speculate that outmost trajectories of collided particles become consistent with path II as U_b becomes large (R_d~>1800, estimated by the varying tendencies of η and U_b), and the collision efficiency tends to be a small constant and only depends on length scale of the stem and particle.

4.2. Retention time

When processing the particle trajectories using Eq. (18), the measured retention time can be obtained. The retention time of a collision-free particle subject to temporal and spatial heterogeneity of the surface velocity around the stem was short enough to be ignored. Recorded particle trajectories within the array of stems were also divided into two segments, delayed (due to stem collision) and smooth transport segments (see Fig. 5). However, this finding cannot apply to particles where

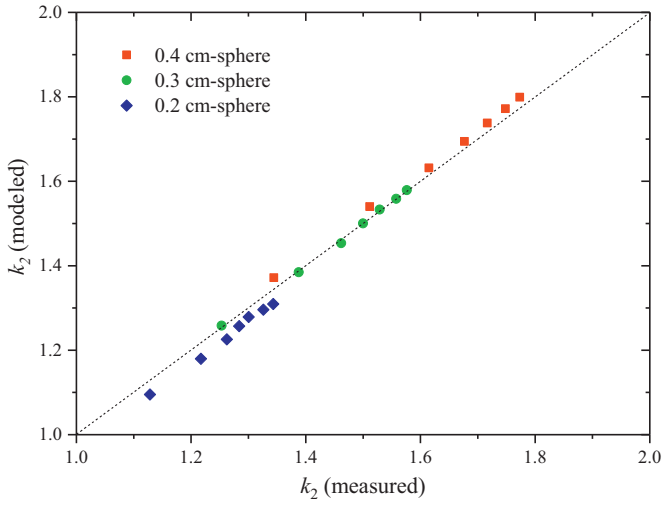

Fig. 9. Comparison between modeled (equation 20) and measured k_2.

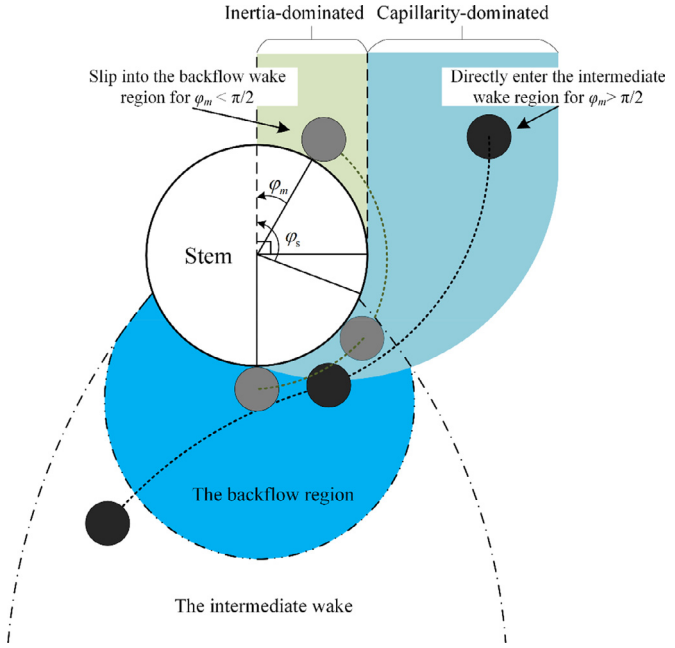

Fig. 10. Varying transport velocity deficits the particle will experience for inertia-dominated and capillarity-dominated outmost trajectories.

capture events due to capillarity cannot be negligible. For downstream floating particles, the retention time of an isolated collision event depends on the collision angle, φ, defined as the angle between the line connecting initial collision point and the center of the stem and the flow direction, and the maximum of which, φ_m (corresponding to the outmost trajectory leading to collision), determines the scale of the retention time distribution (see Fig. 10), and a larger φ_m denotes a greater transport velocity deficit the particle experiences.

When the particle is attracted toward the stem due to surface tension at low-velocity, collision angle φ ranges from 0 to π and $\varphi_m > \pi/2$, the particle will slip into the backflow region and the retention time varies substantially. Defina and Peruzzo (2012) suggested that the distribution of retention time was exponential and divided this distribution into long and short parts, and the proportion of long parts decreases with decreasing flow velocity, for which we speculate the delineating factor for the two parts was the separation angleϕ_s. That is, $\phi < \phi_s$was associated with the long part, where the inelastic collided particle will slip into the backflow wake region under the action of the shear flow and lossless surface tension, and be trapped in the form of quasiperiodic vibration, and the opposite was true for the short part, where the particle enters the intermediate wake region along the edge of the backflow under the action of the backflow and lossy surface tension. With the flow velocity increasing, the inertia effect of the particle becomes dominant ($R_d > 300$) and φ_m gradually reduces to$\varphi_m < \pi/2$. At this point, the retention time is attributed to mechanical collision and transport velocity deficit in the wake. With short retention time of a collision-free particle ignored, the distribution of retention times has a short tail concentrated at the mean valueτ_0. As discussed in section 2.3, $\tau_0$is proportional to the velocity deficit U_f in the wake, and the bulk drag force due to the stem is associated with U_f. The drag coefficient C_{ds} for emergent vegetation has been extensively studied (e.g., Schlichting and Gersten, 1982; Kothyari et al., 2009; Liu and Zeng, 2017). Liu and Zeng (2017) collected and analyzed data from the literature and suggested that C_{ds} depends on R_d and proposed an empirical formula with other factors fixed.

As shown in Fig. 11, τ_0 exponentially decreases with increasing R_d in a manner similar to relations between parameter $C_{ds}a_s/U_b$and R_d with C_{ds} proposed by Liu and Zeng (2017). These findings are consistent with the prediction in Section 2.3 (as the dotted line shown in Fig. 11), the

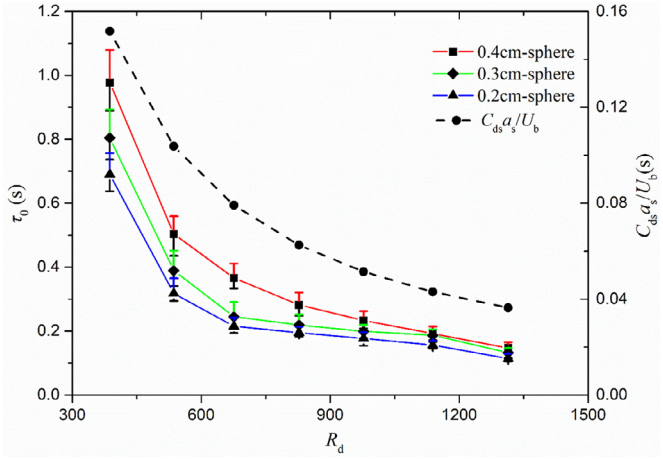

Fig. 11. Variations of the mean retention time $\tau_0$and parameter$C_{ds}a_s/U_b$with the R_d. The vertical error bars represent the variation of measured data.

more massive particle will take longer time in an isolated collision event under the similar flow velocity, i.e., τ_0(0.4 cm) > τ_0 (0.3 cm) > τ_0 (0.2 cm), they require a longer time to regain the mean transport velocity once it is slowed down or arrested by the stem. With further data processing, $\tau_0$appears to be positively related to the retention parameter $(C_{ds}a_s/U_b)(\rho_r/a_r)$ (see Fig. 12).

However, there is an exception for R_d = 387, attributed to the effect of surface tension on trapped particle still exist. As already reported (Peruzzo et al., 2012; Peruzzo et al., 2016; Liu et al., 2018), the capture probability was estimated as the order of magnitude of 10^{-2} for R_d > 500, thereby the effect of surface tension on isolated capture event can be ignored. Particles are observed to be permanently captured (τ_0 > 10 min) for R_d =387 case (Run *B1*). The linear relation between $(C_{ds}a_s/U_b)(\rho_r/a_r)$ and τ_0 after eliminating outliers can be described as

$$\tau_0 = 3.215(C_{ds}a_s/U_b)(\rho_r/a_r) + 0.034 \quad (21)$$

with R^2 = 0.93.

In the present experiments, the measured U_p within the stem density n_s=1366 m^{-2} is significantly greater than U_b consistent with the blockage effect, and considering U_p = 0when U_b = 0, U_p can be described by a linear function with zero intercept, as shown in Fig. 13, U_p of low flow velocity (*A1* and *A2*) does not well conform with the linear

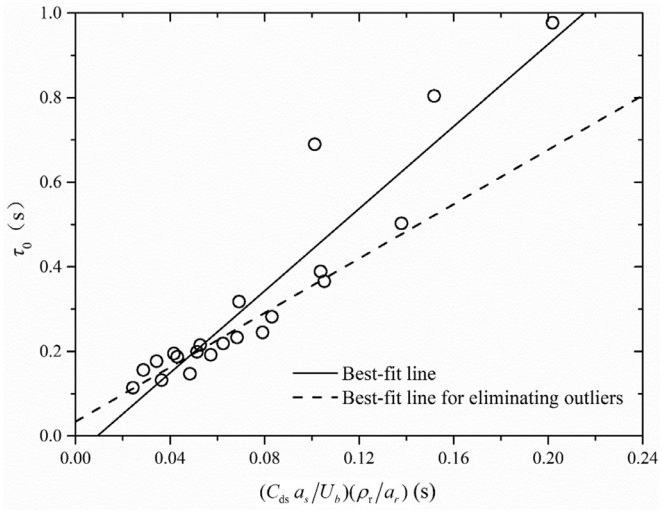

Fig. 12. Variation of the mean retention time$\tau_0$with the retention parameter $(C_{ds}a_s/U_b)(\rho_r/a_r)$.

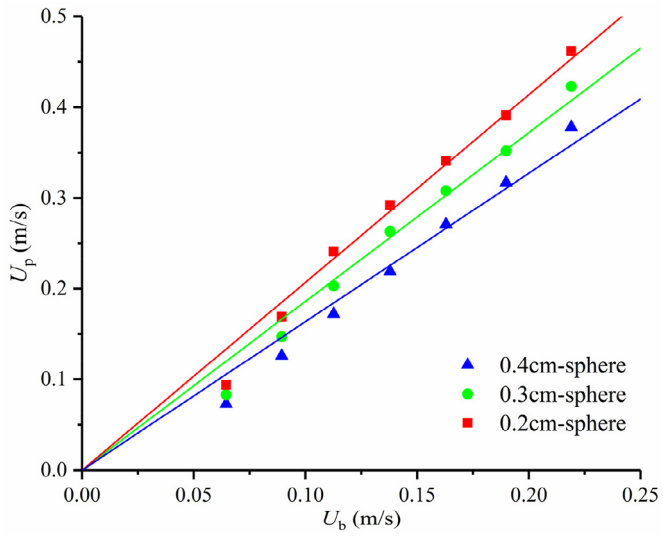

Fig. 13. The measured particle transport velocities of different sizes are plotted as function of U_b with linear fitting lines with zero intercept.

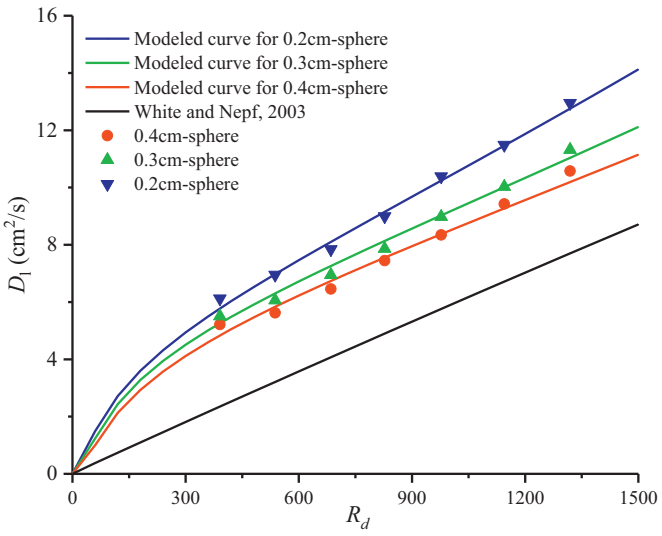

Fig. 15. Variation curve of modeled longitudinal dispersion coefficient D_l and experimental data of present study with R_d for three particle sizes. The dispersion coefficient of White and Nepf (2003) is plotted as a contrast.

relationship, this is because the decelerating effect of surface tension compared with the "blockage effect" on downstream particle can not be ignored, though, the linear relationship for moderate to high flow velocity is acceptable with eliminating outliers for low flow velocities. The slope of relationship curves decreases as a_p increasing, smaller particles are more sensitive to the blockage effect and may obtain greater transport velocity, the reason for which is the smaller moves along the preferential path with higher lateral average constricted cross-section velocity.

After collision with a stem, particles move into the intermediate wake region, the lateral velocity induced by stems will drive particles out of the intermediate wake and then into the free stream. The presence of the stem results in a local increase in the velocity around it, and a streamwise velocity gradient in lateral direction is generated, which results in particles having a preference for drifting toward the higher flow regions among stems due to the lateral pressure difference. Therefore, the measured U_p will be significantly greater than U_b, and affected by stems density. Another reason may be due to the free surface velocity being slightly larger than the depth averaged velocity. As shown in Fig. 14, the increment between particle transport and bulk flow velocity, $\Delta U = U_p - U_b$is larger for smaller floating particles, i.e., the smaller particle is more sensitive to the blockage effect under the similar density. Moreover, ΔU is noticed positively correlated to the stem density (Fig. 14) and can be reasonably fitted by a power relation,

$$\Delta U = 244\lambda^{1.88}U_b \tag{22}$$

with $R^2 = 0.998$.

In fact, the decrement of particle transport velocity due to collision is significantly less than the increment due to the blockage effect; ΔU will steadily increase as λ increases until the center-to-center space between adjacent stems is approximately less than $4a_p$.

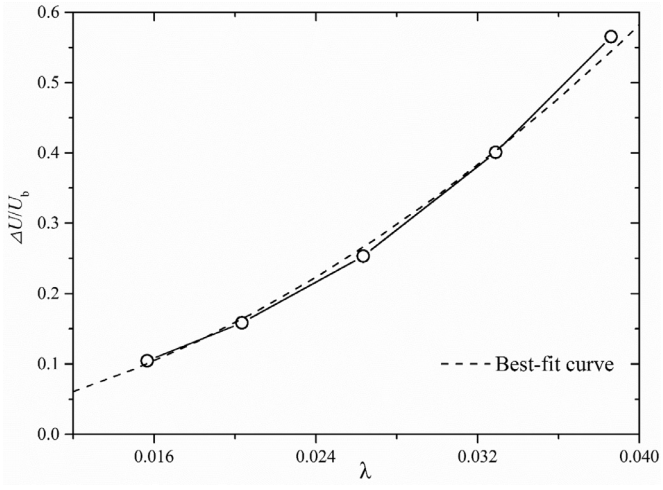

Fig. 14. Variation of the increment velocity ΔU with varying stem densities of λ.

4.3. Longitudinal dispersion coefficient

Within the array of emergent stems, stem-scale and depth-scale dispersion dominate the total longitudinal dispersion, and the motion of floating particles stays in the horizontal plane, depth-scale dispersion can be ignored. The magnitude of longitudinal dispersion within vegetated canopies has been very well studied (e.g., Nepf et al., 1997; White and Nepf, 2003; Lightbody and Nepf, 2006). For sparse canopies (λ<0.1), stem-scale dispersion results primarily from velocity heterogeneity due to the presence of stems, and White and Nepf (2003) the corresponding dispersion coefficient as

$$K_l = \frac{1}{2}C_D^{1/3}U_b d_s \tag{23}$$

for denser canopies ($\lambda > 0.1$), stem-scale dispersion will be dominated by the trapping and release of mass within the boundary-layers and wakes of individual cylinders. Murphy (2006) approximated the stem-scale dispersion at $R_d > 40$ by

$$K_l \cong 5\lambda U_b d_s \tag{24}$$

In present work, the derivation process of D_l is built on spherical particle, moreover, the irregularity of particles and corresponding kinetic difference are taken into consideration in the form of parameters (δ_a, δ_v, γ and S_{tf}), thus, the model can be generalized to seed particles in nature.

Combining the semiempirical formulas of $\tau_0$and η with Eq. (4), the longitudinal dispersion coefficient D_l can be semiempirically modeled and plotted as a function of R_d (ranges from 0 to 1500) in Fig. 15, and can well describe the experimental data. The stem density adopted in this study is less than 0.1, the corresponding dispersion coefficient of

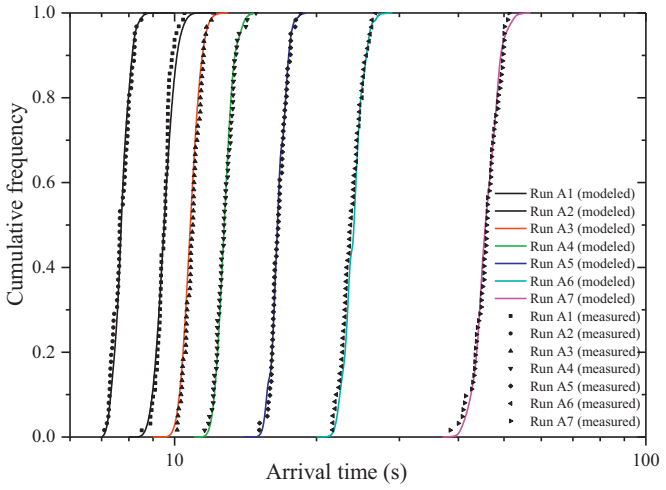

Fig. 16. Cumulative arrival time distributions: Comparison between measured (scatter)

Eq. (23) is also plotted in Fig. 15. As shown in Fig. 15, the dispersion coefficient of solute particles (Eq. 23) is significantly smaller than dispersion coefficient of floating particles, the root of this difference is various dynamic characteristics of particle, and applying mechanically the dispersion coefficient of solute particles to dispersal model of floating seeds is not appropriate. Within the Eulerian framework, the time spent by particles from 0.5m downstream of the front end of the vegetated test section to reach the fixed cross sections (3.5m) and we use these data to construct the cumulative arrival-time distributions, which is used to validate the model, Fig. 16 shows comparison between measured and modeled results of cumulative arrival time distributions for Runs A1-A7, the results are satisfactory. The D_l increases with an increase in R_d, which may be due to the contribution of mechanical dispersion becoming weaker with increasing U_b, and the delayed transport in wake region behind the stem becoming dominant. Moreover, D_l deserves a higher value for smaller particles, however, $\tau_0$and η become much less for small particles, we can surmise that D_l of floating particles is more sensitive to the blockage effect. With the increase in stem density, the increment of η and U_p becomes more significant than the decrement in C_{ds} from the wake interference or sheltering (Nepf, 1999). Hence, D_l increases with stem density due to more effective mechanical dispersion and this issue deserves future investigation. Through the proposed semiempirical model of longitudinal dispersion, the rules of transport of floating seeds in vegetated aquatic flows can be investigated, and we suggest that the results are of great significance to ecological restoration or restoration of riparian and wetland systems, harnessing farmland weeds and even preventing invasion of exotic aquatic plant species, especially for riparian, aquatic, and wetland systems. and modeled results (full line).

5. Conclusions

Two key mechanisms responsible for floating particle dispersal in fast-moving flow within emergent vegetation have been studied. These mechanisms include collisions between a particle and stems (mechanical dispersion) and subsequent wake trapping effect (wake turbulence dispersion). These two mechanisms differ from previous studies in slow-moving flow where surface tension played a leading role in particle capture by vegetation. A theoretical model of longitudinal dispersion based on a collision representation with appropriate length scales is proposed to describe the downstream transport process of floating seeds within the array of stems. The model leads to an algebraic expression between longitudinal dispersion, collision efficiency η between particles and the stem and retention time τ_0. For usability, parameterizing η and retention time as a function of flow variables such as bulk velocity, canopy properties and particle physical properties are necessary. The kinematic model is established with potential flow theory to predict the collision efficiency between the particle and the stem to a first approximation.

The overall time particles reside in the wake is defined on the basis of an isolated collision event, and shown to be positively correlated with the bulk drag coefficient and relative radius of stems using a simplified wake theory. The distribution of retention times was shown to be related to the collision angle, which may explain the superposition of two-distribution relations proposed by Defina and Peruzzo (2012). The increment between particle transport and bulk flow velocity has a positive correlation with the blockage effect among stems, and increases exponentially with increased stem density, beside, smaller particles can be considered more sensitive to the blockage effect and obtain greater transport velocity. By comparison, present semiempirical formula of D_l can well describe the experimental data, and the dispersion coefficient of solute particles is significantly smaller than dispersion coefficient of floating particles, the root of the difference is various dynamic charateristics of particle. To pursue the collision events further, only a dense stems array ($n_s = 1366\ m^{-2}$) was used for the dispersal process, which means that the effect of stem density on the retention time is not varied. Increasing λ influences C_{ds} as expected as well as the width of the wake (Zdravkovich, 1997). Thus, further studies on the dependence of λ on τ_0 are needed, and the application of the present theoretical model will be further evaluated in future studies.

Declaration of Competing Interest

The authors declare that they have no known competing financial interests or personal relationships that could have appeared to influence the work reported in this paper.

The authors declare the following financial interests/personal relationships which may be considered as potential competing interests:

CRediT authorship contribution statement

Xiaoguang Liu: Conceptualization, Methodology, Formal analysis, Resources, Investigation, Writing - original draft, Writing - review & editing, Validation. **Yuhong Zeng:** Methodology, Formal analysis, Writing - review & editing, Supervision, Funding acquisition, Project administration. **Gabriel Katul:** Methodology, Formal analysis, Writing - review & editing, Supervision. **Wenxin Huai:** Formal analysis, Writing - review & editing. **Yu Bai:** Writing - review & editing.

Acknowledgment

Y. Zeng acknowledges support from National Natural Science Foundation of China (51879197,51622905 and 51439007), and support from the Overseas Expertise Introduction Project for Discipline Innovation (111 Project) funded by Ministry of Education and State Administration of Foreign Experts Affairs P.R. China (B18037).

G. Katul acknowledges support from the U.S. National Science Foundation (NSF-AGS-1644382 and NSF-IOS-1754893).

References

Britter, R., Hunt, J., Mumford, J., 1979. The distortion of turbulence by a circu-lar cylinder. J. Fluid Mech. 92 (2), 269–301.
Clark, J.S., Macklin, E., Wood, L., 1998. Stages and spatial scales of recruitent limitation in southern Appalachian forests. Ecol. Monogr. 68 (2), 213–235.
Cunnings, A., Johnson, E., Martin, Y., 2016. Fluvial seed dispersal of riparian trees: transport and depositional processes. Earth Surf. Process. Landf. 41 (5), 615–625.
Danvind, M., Nilsson, C., 1997. Seed floating ability and distribution of alpine plants along a northern Swedish river. J. Veg. Sci. 8 (2), 271–276.
Defina, A., Peruzzo, P., 2010. Floating particle trapping and diffusion in vegetated open channel flow. Water Resour. Res. 46 (11).
Defina, A., Peruzzo, P., 2012. Diffusion of floating particles in flow through emergent vegetation: further experimental investigation. Water Resour. Res. 48 (3).

DeWoody, J., Nason, J.D., Smith, M., 2004. Inferring demographic processes from the genetic structure of a metapopulation of Boltonia decurrens (Asteraceae). Conserv. Genet. 5, 603–617.
Duman, T., Trakhtenbrot, A., Poggi, D., Cassiani, M., Katul, G.G., 2016. Dissipation intermittency increases long-distance dispersal of heavy particles in the canopy sublayer. Bound. Layer Meteorol. 159 (1), 41–68.
Di Carlo, D., J.F., Edd, Humphry, K.J., Stone, H.A., Toner, M., 2009. Particle segregation and dynamics in confined flows. Phys. Rev. Lett. 102 (9), 094503.
Fischer, H.B., 1973. Longitudinal dispersion and turbulent mixing in open-channel flow. Ann. Rev. Fluid Mech. 5 (1), 59–78.
Greene, D., Johnson, E., 1996. Wind dispersal of seeds from a forest into a clearing. Ecology 77 (2), 595–609.
Groves, J.H., Williams, D.G., Caley, P., Norris, R.H., Caitcheon, G., 2009. Modelling of floating seed dispersal in a fluvial environment. River Res. Appl. 25 (5), 582–592.
Hyslop, J., Trowsdale, S., 2012. A review of hydrochory (seed dispersal by water) with implications for riparian rehabilitation. J. Hydrol. (N. Z.) 137–152.
Katul, G., Li, D., Manes, C., 2019. A primer on turbulence in hydrology and hydraulics: the power of dimensional analysis. Wiley Interdiscip. Rev.: Water 6 (2), e1336.
Katul, G., Porporato, A., Nathan, R., Siqueira, M., Soons, M., Poggi, D., Levin, S.A., 2005. Mechanistic analytical models for long-distance seed dispersal by wind. Am. Nat. 166 (3), 368–381.
Kiya, M., Tamura, H., Arie, M., 1980. Vortex shedding from a circular cylinder in moderate-reynolds-number shear flow. J. Fluid Mech. 101 (4), 721–735 528.
Kothyari, U.C., Hashimoto, H., Hayashi, K., 2009. Effect of tall vegetation on sediment transport by channel flows. J. Hydraul. Res. 47 (6), 700–710.
Levine, J.M., 2003. A patch modeling approach to the community-level consequences of directional dispersal. Ecology 84 (5), 1215–1224.
Lightbody, A.F., Nepf, H.M., 2006. Prediction of velocity profiles and longitudinal dispersion in salt marsh vegetation. Limnol. Oceanogr. 51 (1), 218–228.
Liu, X., Zeng, Y., 2017. Drag coefficient for rigid vegetation in subcritical open-channel flow. Environ. Fluid Mech. 17 (5), 1035–1050.
Liu, X., Zeng, Y., Huai, W., 2018. Modeling of interactions between floating particles and emergent stems in slow open channel flow. Water Resour. Res. 54 (9), 7061–7075.
Liu, Xiaoguang, Zeng, Yuhong, Huai, Wenxin, 2019. Floating seed dispersal in open channel flow with emergent vegetation. Ecohydrology 12 (1).
Maskell, E., 1963. A theory of the blockage effects on bluff bodies and stalled wings in a closed wind tunnel (Tech. Rep.). Aeronaut. Res. Council Lond. (U. K.).
Merritt, D.M., Wohl, E.E., 2006. Plant dispersal along rivers fragmented by dams. River Res. Appl. 22 (1), 1–26.
Murphy, E., 2006. Longitudinal dispersion in vegetated flow (doctoral dissertation. Mass. Inst. Technol.).
Nathan, R., Katul, G.G., Bohrer, G., Kuparinen, A., Soons, M.B., Thompson, S.E., Horn, H.S., 2011. Mechanistic models of seed dispersal by wind. Theor.l Ecol. 4 (2), 113–132.
Nathan, R., Katul, G.G., Horn, H.S., Thomas, S.M., Oren, R., Avissar, R., Levin, S.A., 2002. Mechanisms of long-distance dispersal of seeds by wind. Nature 418 (6896), 409.
Nepf, H., 1999. Drag, turbulence, and diffusion in flow through emergent vegetation. Water Resour. Res. 35 (2), 479–489.
Nepf, H., Mugnier, C., Zavistoski, R., 1997. The effects of vegetation on longitudinal dispersion. Estuar. Coast. Shelf Sci. 44 (6), 675–684.
Nilsson, C., Brown, R.L., Jansson, R., Merritt, D.M., 2010. The role of hydrochory in structuring riparian and wetland vegetation. Biol. Rev. 85 (4), 837–858 558.
Nilsson, C., Ekblad, A., Dynesius, M., Backe, S., Gardfjell, M., Carlberg, B., Jansson, R., 1994. A comparison of species richness and traits of riparian plants between a main river channel and its tributaries. J. Ecol. 562, 281–295.
Okubo, A., Levin, S.A., 1989. A theoretical framework for data analysis of wind dispersal of seeds and pollen. Ecology 70 (2), 329–338.
Palmer, M.R., Nepf, H.M., Pettersson, T.J., Ackerman, J.D., 2004. Observations of particle capture on a cylindrical collector: Implications for particle accumulation and removal in aquatic systems. Limnol. Oceanogr. 49 (1), 76–85.
Peruzzo, P., Defina, A., Nepf, H., 2012. Capillary trapping of buoyant particles within regions of emergent vegetation. Water Resour. Res. 48 (7).
Peruzzo, P., Viero, D., P.and Defina, A., 2016. A semi-empirical model to predict the probability of capture of buoyant particles by a cylindrical collector through capillarity. Adv. Water Resour. 97, 168–174.
Riis, T., Sand-Jensen, K., 2006. Dispersal of plant fragments in small streams. Freshw. Biol. 51 (2), 274–286.
Rutherford, J.C., 1994. River Mixing. Wiley, New York.
Schneider, R.L., Sharitz, R.R., 1988. Hydrochory and regeneration in a bald cypress-water tupelo swamp forest. Ecology 69, 1055–1063.
Shi, W., Shao, D., Gualtieri, C., Purnama, A., Cui, B., 2020. Modelling long-distance floating seed dispersal in salt marsh tidal channels. Ecohydrology 13 (1), e2157.
Thom, A., 1933. The flow past circular cylinders at low speeds. Proceed. R. Soc. Lond. Ser. A 141 (845), 651–669.
White, B.L., Nepf, H.M., 2003. Scalar transport in random cylinder arrays at moderate Reynolds number. J. Fluid Mech. 487, 43–79.
Zavistoski, R.A., 1994. *Hydrodynamic Effects of Surface Piercing Plants*. Unpublished Doctoral Dissertation. Massachusetts Institute of Technology.
Zdravkovich, M., 1997. Flow around circular cylinders; volume 1. fundamentals. J. Fluid Mech. 350, 377–378.
Ziemniak, E.M., Jung, C., Tél, T., 1994. Tracer dynamics in open hydrodynamical flows as chaotic scattering. Phys. D: Nonlinear Phenom. 76 (1-3), 123–146.